# THERMAL-HYDRAULIC ANALYSIS OF LIGHT WATER REACTORS UNDER DIFFERENT STEADY-STATE OPERATING CONDITIONS Part 2 – Pressurized Water Reactor

by

***Ezddin HUTLI*** [1] ***and Ramadan KRIDAN*** [2]

[1] Institute of Nuclear Techniques, Budapest University of Technology and Economics, Budapest, Hungary
[2] Department of Nuclear Engineering, Faculty of Mechanical Engineering, University of Tripoli, Tripoli, Libya

Scientific paper
https://doi.org/10.2298/NTRP2204276H

**The 1-D computer code MITH was used in this paper to perform sub-channel thermal-hydraulic analyses of a typical (Westinghouse model) pressurized water reactor. Two typical channels, hot and average, with the same flow rate and pressure drop, were tested under steady-state operating conditions. In this analysis, the channel with the highest temperature is designated as the hot channel. For the calculations, the channel model was divided into 20 parts. The thermal-hydraulic performance of the tested reactor was affected by power distribution, power level, and coolant mass-flow rate. Temperature distribution profiles of the fuel element and coolant are obtained for the average and hottest channels. A critical heat flux $q_{cr}$ analysis is also carried out and the heat fluxes in both channels were calculated. The W-3 correlation is employed to examine $q_{cr}$ in the hottest channel. Some data from the pressurized water reactor typical data sheet were used as input data, while others were used to validate the code. The code faithfully reproduced the Westinghouse model reactor results, including coolant, cladding, centerline, and surface fuel temperatures, quality and local heat flux $q_{loc}$, $q_{cr}$, and minimum departure from nucleate boiling ratio.**

*Key words: fuel, clad, coolant, temperature, pressure, heat flux, departure from nucleate boiling ratio*

## INTRODUCTION

The reactor core is a critical component of a nuclear reactor that generates heat and displays the highest temperatures. Temperatures in the reactor core must be predicted for a variety of reactor operating conditions. Temperatures must be kept below specific thermal limit values for various reactor constructions and fuel materials to ensure safe reactor operation. The specific limitation is that the core temperature components must remain below the melting points of the materials used, primarily the fuel and cladding materials. The limits are extended to the heat transfer rate between the fuel elements and the coolant, because the $q_{cr}$ may be approached, resulting in a phase change and partial film coverage of the clad surface. As a result, the cladding's temperature will rapidly rise.

In the nuclear reactor design stage, neutron and thermal-hydraulic calculations must be validated to ensure that the thermal limits – the melting temperatures of the fuel and cladding, as well as the MDNBR are within the specified limit [1].

In practice, the limit of the core operational power is determined by a thermal-hydraulic study, calculation and analysis that determines the operational condition to avoid structural and fuel deterioration. To keep the core intact, the fuel, cladding, and coolant temperatures, as well as the surface heat flux, must stay within the proposed design limits [2-5].

The heat produced in nuclear reactors has an impact on the core structure and the nuclear reaction process. Under normal operating conditions, the heat produced causes variations in the temperatures and densities of the core materials, causing the reaction rate to change as a result. These variations have an impact on the balance of neutron production and destruction. Power and reactivity temperature coefficients could indicate the impact of these variations. These two variables are critical for detecting reactor behavior [1, 3].

The goal of a reactor core's thermal-hydraulic safety analysis, as is well known, is used to achieve adequate heat transfer compatible with the core's power distribution under various steady-state and transient operating conditions and controlling the clad and fuel temperatures to maintain them below their melting points as will as to maintain the coolant conditions unchanged [6]. One of the specified safety limits in pressurized water reactor (PWR) is the departure from nucleate boiling ratio (DNBR). It is the ratio of the critical heat flux (CHF) $q_{cr}$ that causes departure from

* Corresponding author, e-mail: ezddinhutli@yahoo.com

nucleate boiling (DNB) phenomenon to the actual local heat flux $q_{act}$ in the hottest channel, this ratio represents the margin against DNB. To preserve the fuel element, the $q_{cr}$ should be greater than the maximum heat flux that created in the hot channel $q_{act}$. The DNB is a critical phenomenon that must be avoided, it is a complex phenomenon influenced by a variety of physical factors, including the design of the fuel assembly and the distances between the fuel rods [7, 8].

Since PWR use only liquid phase coolant, the $q_{cr}$ is the main issue that needs to be controlled from a reactor safety perspective. When a certain wall heat flux is exceeded, the rate of heat transfer gradually decreases because of the phase change process that produces a vapor film on the surface; when the film appears, the rate of heat transfer dramatically decreases [9].

Thermal hydraulics has played an important role in the design, operation, performance, and safety of nuclear power plants since the 1950 s [10]. Global research and development (R&D) have significantly improved the design, operation, and performance of nuclear power reactors, as well as our understanding of thermal hydraulics. Increased coolant flow rates improve heat transfer coefficients and allow for higher limits of $q_{cr}$ due to the mixing process between the sub-channels and the changing velocity distribution in the flow area. Higher flow rates, on the other hand, will result in larger pressure drops across the core, necessitating larger pumping powers, which will result in higher dynamic loads on the core components and vibrate the fuel elements. The prediction of velocity distribution and the evaluation of thermal-mixing performance are essential in nuclear fuel assembly design and thermal-hydraulic analysis. The pressure drops and velocity distributions in the sub-fuel assembly, which help predict the mixing process, the mass-flow rates situation, and the coolant temperature profile are the main parameters to be evaluated. The mechanisms of the mixing process in the fuel assemblies are depicted as a cross and swirl flow between and within the sub-channels. The mixing is required first to improve the heat transfer process, which allows the reactor's operating power to be increased, and second to obtain a uniform outlet temperature profile for the reactor's performance, for this purpose, the spacer grids associated with mixing vanes are taken into account during the fuel assembly design stage; the spacer grids primarily serve as a fixer and supporter to the fuel elements. In a nuclear power plant, optimal heat removal from the surface of nuclear fuel elements is essential for reactor thermal and safety margins. To have a uniform inlet temperature profile, the mixing phenomenon as a process is also important in the primary loop of the coolant. In the case of a loss of coolant accident (LOCA), mixing is also required; more information on the importance of the mixing phenomenon for nuclear reactors in steady-state and accident conditions can be found in the literature [11-17].

The use of a code for thermal-hydraulic analysis is widely accepted as the framework for nuclear power plant design and safety analysis. Because conducting experiments in this field is prohibitively expensive, computer codes are used to analyze the thermal-hydraulics of various reactor parts under various operating conditions. The codes use basic equations from fluid mechanics and heat transfer, such as the continuity, momentum, and energy transfer equations, to accomplish this task. Significant efforts have been made over the last four decades to provide reliable thermal-hydraulic system codes for the analysis of transients and accidents in nuclear power plants. There are three methods for analyzing the thermal-hydraulics of the reactor core. The first is the single-channel method, and the second is the subchannel method. These methods have been used since the 1970 s, and a third method, which analyzes parallel channel three- dimensional data, was recently introduced. The averaged channel thermal-hydraulic behavior is obtained using the single-channel analysis code. To solve conservation equations, the sub-channel method is commonly used [17, 18].

Because mixing flow is involved, sub-channel codes provide more accurate modeling of the entire reactor core or a single assembly than single-channel codes. To reduce the massive computational costs, detailed pin-by-pin sub-channel modeling of an entire core must be run in parallel. Many codes, including RELAP5, COBRA-EN, and CTF [19-21], use such models to accurately simulate the thermal-hydraulics process. In addition to the codes mentioned, there are others available, such as COBRA-3C/RERTR, PARET, and COOLED-N. The COBRA and THINC codes are the most commonly used for these purposes [22-24]. The accuracy and adaptability of the codes and methods used in the design and analysis stages are essential for nuclear power plant safety and cost-effectiveness. The high precision numerical reactor simulations that include all relevant reactor physics requirements are also required [25, 26].

To understand the relationship between the main parameters that affect the thermal-hydraulic performance of PWR, MITH, a simplified thermal-hydraulic computer code, was employed in this study. its sub-channel code for steady-state operating conditions. It was written in Fortran and provides axial and radial temperature distributions, as well as DNBR distributions and other hydraulic calculations such as pressure drop, all, while accounting for the reactor core's average and hottest channel. The W-3 correlation was used for these calculations, with the type of reactor taken into account. In this work, a typical PWR(W) (W among the brackets indicates the Westinghouse company producer) with uranium oxide ($UO_2$) fuel is used as a case study, with other typical reactor data presented in tab. 1 [27]. To validate the code, the obtained results were compared to the thermal limits and safety parameters specified in the tested reactor's technical data sheet, as well as the general thermal-hydraulic constraints of PWR [1]. The code and results obtained for the tested PWR are described. The description of the applied code is presented in Hutli and Kridan (2022/2023) [3]. The

**Table 1. The input parameters for a typical PWR case study (Westinghouse design) [27]**

| General data | Value | Fuel assemblies | Square |
|---|---|---|---|
| | | Assembly pitch [cm] | 21.5 |
| | | Assembly dimension [$cm^2$] (Horizontal cross-section) | 21.4 21.4 |
| | | Number of fuel /assembly | 264 |
| Thermal output [MW] | 3411 | Total number of fuel locations | 501952 |
| Electrical output [MW] | 1150 | Fuel element O.D. [cm] | 0.95 |
| Efficiency $\varepsilon$ [%] | 33.7 | Pitch/diameter | 1.32 |
| Fuel type | $UO_2$ | Clad thickness [cm] | 0.0572 |
| Coolant | $H_2O$ | Fuel-pellet diameter [cm] | 1.819 |
| Structural material (cladding) | Zircaloy-4 Zirconium alloy | Pellet-clad gap [cm] | 0.0082 |
| Moderator | $H_2O$ | Fuel enrichment | 2.1/2.6/3.1 |
| Core data | | | |
| Active height [cm] | 366 | Thermal-hydraulic data | |
| Equivalent\active diameter [cm] | 377 | System pressure (bar) | 155 |
| Height/diameter | 1.09 | | |
| Active core volume (L) | 32800 | Coolant flow [$10^6$ $kgh^{-1}$] | 62 |
| Average core power density [$kwL^{-1}$] | 104 | Average linear power density [$Wcm^{-2}$] | 178 |
| Fuel weight [kg] | 90200 | Maximum linear power density [$Wcm^{-1}$] | 426 |
| Specific power [$kW/kgU^{-1}$] | 37.8 | Average heat flux [$Wcm^{-2}$] | 68.5 |
| Burnup [MWd/tU] | 33000 | Maximum heat flux [$Wcm^{-2}$] | 183 |
| Conversion ratio | 0.5 | Minimum DNBR | 13 |
| Fuel assembly type | Square bundle | Inlet temperature [°C] | 1.3 |
| Number of fuel assemblies | 193 | Outlet temperature [°C] | 332 |
| Fuel elementary array | 17 17 | Maximum fuel temperature [°C] | 1788 |

flowcharts of the code and the channel model are shown in figs. 1(a) and 1(b).

## CODE INPUT DATA

The input data are; thermal power output (MW), mass flow rate [$kgh^{-1}$], coolant inlet temperature [°C], inlet pressure (bar, 1 bar = 100 kPa), number of fuel rods, the outer diameter of fuel rod [cm], clad thickness [cm], unheated upper channel part [cm], unheated lower channel part [cm], pitch type, rod pitch [cm], active channel length [cm], number of a discrete interval, the form factor for spacer grids, profile power distribution, and radial number hot channel factor. Also the thermal conductivity of fuel, $UO_2$, (0.0294 $Wcm^{-1}(°C)^{-1}$, the thermal conductivity of cladding, Zircaloy-4 alloy, 0.215 $Wcm^{-1}(°C)^{-1}$, and the heat transfer coefficient of the gas in the gap, Helium 25.94 $Wcm^{-1}(°C)^{-1}$.

## AXIAL POWER DISTRIBUTIONS – COSINE PEAKED

Figure 2(a)-2(d) depicts the effect of power radial peaking factors on the cladding and coolant temperatures, as well as the temperature of the fuel elements (centerline and surface) in the average and hot channels, respectively.

## COOLANT TEMPERATURE

The coolant enters the core at the bottom and flows upwards around the fuel rods, absorbing energy from heat transfer caused by nuclear reactions.

Figure 2(a) depicts the coolant temperature profile along the average and hot channels, respectively. The analysis of the profiles in both channels reveals that the temperature rises during steady-state operation. In the average channel, the coolant temperature rises from 300 °C to 333.59 °C, resulting in an average coolant-heating rate of 33.59 °C. The coolant outlet temperature from the average channel does not differ too much from the core outlet temperature (bulk temperature). Assuming the pressure are equal in all channels of the core, in this channel the coolant temperature did not reach the saturation temperature at the operating pressure (155 bar), which is 345.32 °C. This is a PWR feature, and it means that the coolant temperature is well within the thermal-hydraulic limitations. In PWR, it is necessary to prevent coolant bulk boiling.

The coolant temperature in the hot channel rises from 300 °C at the channel inlet to 345.1 °C at the channel outlet, resulting in a heating rate of 45.1 °C along this channel. As a result, the outlet temperature is equal to the saturation temperature at the core operating pressure, thus the boiling process can begin somewhere along the hot channel and most probably the outlet part. If this temperature is recorded at any

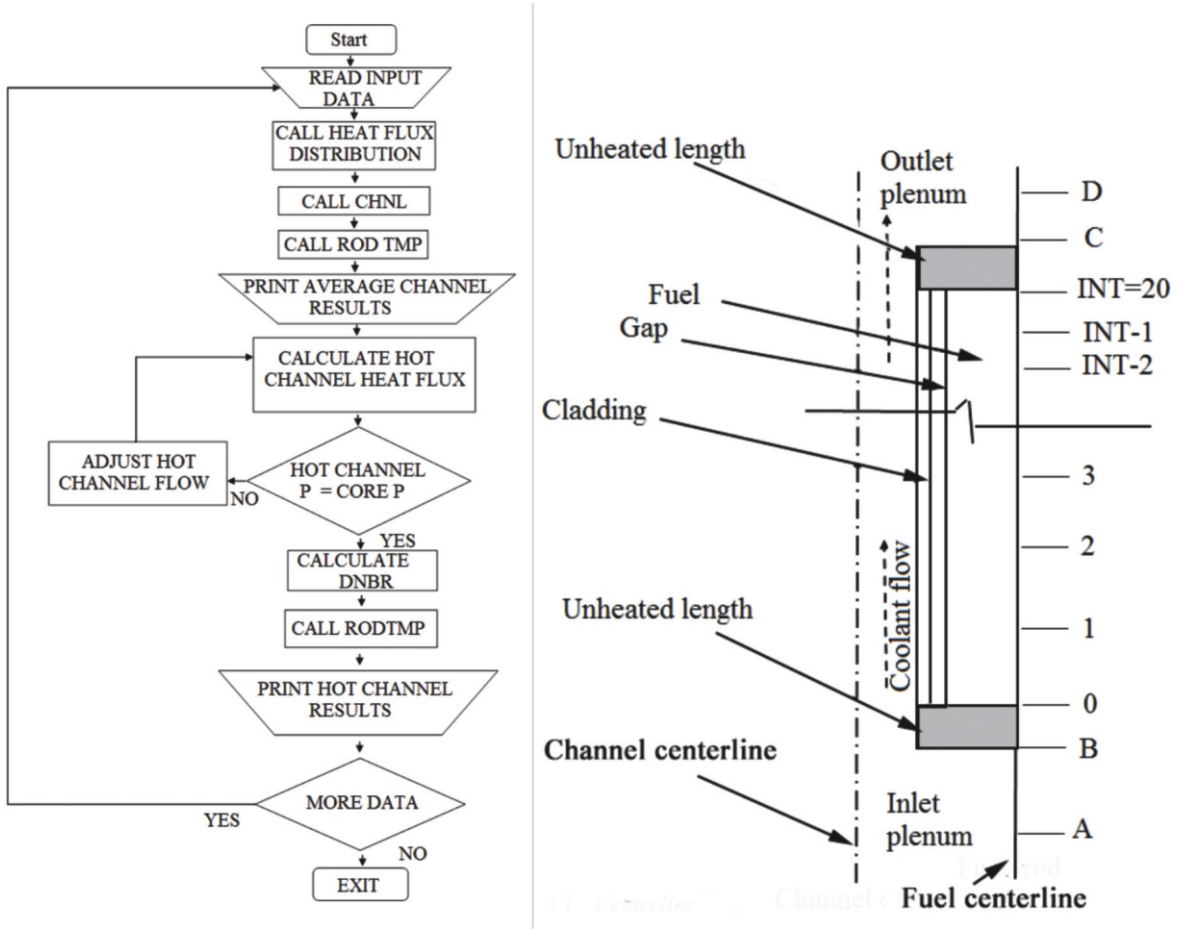


**Figure 1. Flowchart of the code (a) and channel model (b)**

point in the hot channel, it can be used as an indicator of the risk that may appear if reactor power is slightly increased or coolant mass-flow is decreased. In these cases, the boiling process in the channel is expected.

It means that the coolant temperature in this channel is not under the thermal-hydraulic limitations. The fact that the result exceeds the limit in the technical data sheet for a typical reactor tab. 1 may be because the hot channel factor utilized in this calculation is higher than the one used by the designer. This result showed that at the coolant flow rate $62 \cdot 10^6$ kgh$^{-1}$ the pressure drop is below 200 kPa (the pressure drop is discussed at the end of the paper) and the MDNBR above 1.30, but $T_{out}$ at 345.1°C is above its 332 °C limit, tab. 1. Based on this result in order to achieve an operating state for this reactor that satisfies all of these constraints, further sensitivity analysis is required, which involves lowering the core inlet temperature $T_{in}$ from its reference value (300 °C) at a constant mass flux of $62 \cdot 10^6$ kghr$^{-1}$ in order to lower core outlet temperature $T_{out}$ below 332 °C. Anyhow, it is generally important to control the power generated in the hot channel to avoid the occurrence of the $q_{cr}$ and its consequences. This can be achieved by optimizing the relationship: between heat generation and flow rate. There are two ways to optimize the relationship: by lowering power generation or increasing flow rate in the channel.

The difference in heating rates between the two channels is due to the hot channel's higher radial power peaking factors as a consequence of its position in the core.

Higher outlet coolant temperatures are preferred for heat transmission, as is widely documented. Water serves as both a coolant and a moderator in LWR, so two competing mechanisms contribute to density feedback. As a result, increasing the temperature of the coolant has two opposing effects on reactivity. When the temperature rises, the coolant density and boron solubility decrease, while the reactivity increases due to the slower absorption rate process. While decreasing coolant density causes a decrease in the moderation rate process, it also causes a decrease in reactivity [26]. The first effect has a smaller impact on reactivity than the second under normal operating conditions. As a result, increasing the temperature of the coolant causes negative reactivity feedback [1-4, 28-31].

Because the density of water decreases with height, a better moderation process exists in the lower part of the core. As a result, the power generation rate

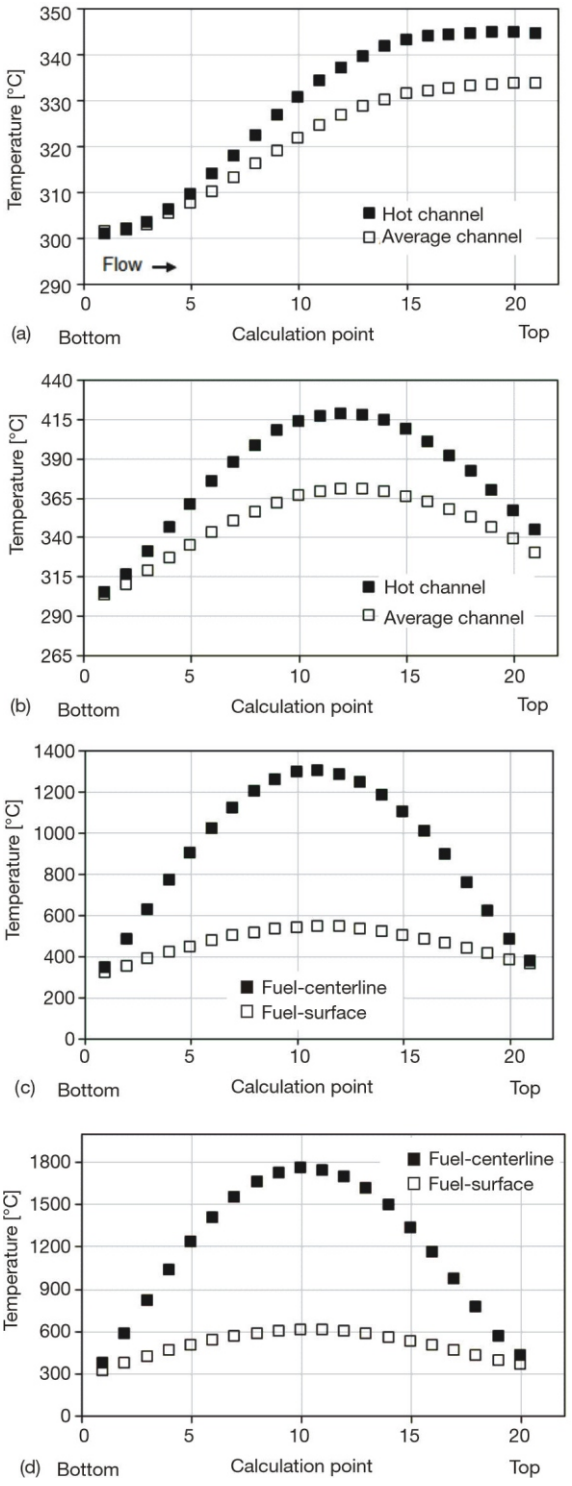


**Figure 2. Axial temperature distribution at nominal power; (a) coolant, (b) cladding outer surface, and (c), (d) fuel in the average and hot channels, respectively, steady-state operation at nominal power, cosine peaked-power distribution**

in the lower part of the core is expected to be higher. As previously stated, it is also expected that the power peak in the axial direction will be reduced by negative reactivity feedback with an increase in power generation rate in the lower part of the reactor core due to the high coolant density in that part of the reactor core [26].

## TEMPERATURES AT THE CENTERLINE, THE FUEL SURFACE, AND THE CLADDING'S OUTER SURFACE

The cladding material is not strictly defined in the data sheet of the tested reactor; a zircaloy was mentioned as structure material without a grade for zircaloy [27]. As well known in PWR, the most widely used cladding has been zircaloy-4 (containing Zr-Sn-Fe-Cr). Although still in use in many PWR, zircaloy-4 is gradually being replaced by Zr-1 % Nb and Zr-2.5 % Nb alloys. Zirconium-niobium alloys containing 1.0 wt.% and 2.5 wt.% niobium have been investigated for use as fuel cladding. Based on that we assumed that the cladding material used in the tested reactor is zircaloy-4 [32]. While the tested reactor's fuel material is defined in the datasheet; the fuel is uranium dioxide ($UO_2$) [27]. The $UO_2$ is assumed as a ceramic refractory uranium compound, usually used as a nuclear fuel. It is a stable ceramic that can be heated almost to its melting point (2878  20 °C), without significant mechanical deterioration. It has no significant reaction with water [33].

Figure 2(b) shows the cladding temperatures in the average and hot channels, respectively. The cladding outer surface temperature in the average channel is equal to the inlet coolant temperature at the channel inlet, then begins to increase with height until it reaches its maximum value of 366.11 °C approximately at half of the channel, then begins to decrease in the second half of the channel until it reaches the coolant temperature at the channel end. Even the acquired temperature profile of the clad's outer surface is not fully identical to the applied power distribution profile, but it is dependent on the power distribution in the core, as we will see later.

The hot channel's cladding temperature profile has the same tendency as the average channel, but the maximum cladding temperature in the hot channel is recorded at the end of the first third of the channel. The highest recorded temperature at the hot channel was 404.27 °C, which is higher than the coolant's saturation temperature, indicating that subcooled boiling can occur. Subcooled boiling is desirable in some cases because it improves heat transfer. Some vapor bubbles form on the surface of the cladding as a result of partial boiling. This type of boiling is known as subcooled boiling in the thermodynamic field. The originated bubbles have high temperatures elaborated from the surface due to the difference in density with its surroundings and due to the continuous movement of the coolant. The heat from these bubbles is transferred to the coolant, which causes them to collapse.

Because the hot channel has larger power peaking factors due to its position in the core, the maximum temperature positions in the channels differ, as well as the time necessary to achieve the maximum tempera-

ture. The maximum cladding temperature difference between hot and average channel factors is 38.16 °C.

According to this result and from the standpoint of reactor safety, it is necessary to regulate the power produced in the hot channel in order to prevent the occurrence of the $q_{cr}$ and its consequences.

Figures 2(c) and 2(d) depict the temperature distribution in the fuel centerline and fuel surface in the average and hot channels, respectively. The temperature profiles for the average channel's fuel centerline and fuel surface fig. 2(c) are similar to the applied power distribution (cosine peaked). Both profiles show that the temperature gradually increased, with the height reaching its peak at 1296.19 °C and 522.91 °C, respectively, at half of the fuel element (channel). Following that, the temperature gradually began to drop to the fuel element's end (channel outlet).

The temperature profiles in the hot channel fig. 2(d) resemble those in the average channel in shape and behavior, but they are higher. Maximum temperatures in the fuel centerline and fuel surface are also calculated, with values at the center of the fuel element of 1772.48 °C and 599.23 °C, respectively. The highest recorded temperature in the hot channel indicates that the fuel temperatures are well within thermal-hydraulic margins.

As is well known, the reactivity coefficients establish the relationship between the power produced by the fuel and the thermo-physical parameters of the fuel and moderator [26, 27]. The temperature of the fuel has a significant impact on the reaction rate in the core as well as the power distribution. As nuclide temperatures change, the Doppler broadening effect changes the cross-sections of the resonance absorption, which has a negative feedback effect on reactivity. As a result, the temperature of the fuel pin has a significant impact on both reactivity and power distribution. Furthermore, the fuel pin temperature has a distinct radial distribution, and the fuel center temperature is significantly different from the fuel surface temperature [24]. Figures 2(c) and 2(d) clearly demonstrate this distinction. In general, fuel pin temperature, coolant temperature, and density all affect basic cross-sections (particularly absorption) and thermal scattering cross-sections. The resonance absorption of the target nuclide with neutrons in specific energy regions varies dramatically with temperature. Because cladding temperature has little effect on neutron absorption, the neutronics and thermal-hydraulics feedback considers only three parameters: fuel temperature, coolant temperature, and density [26].

## AXIAL POWER DISTRIBUTIONS – BOTTOM PEAKED

Figures 3(a)-3(d) depicts the temperature distribution in the cladding outer surface, the coolant, and the fuel centerline and fuel surface in both average and hot channels.

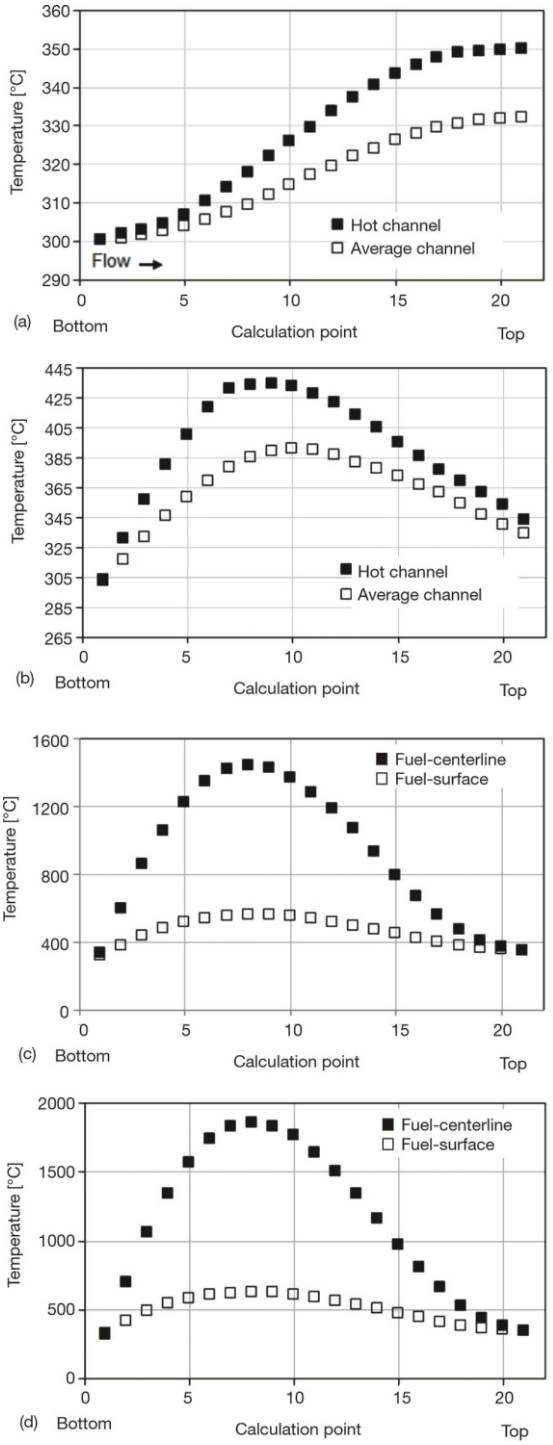


**Figure 3. Axial profile temperature distribution at nominal power; (a) coolant, (b) cladding outer surface, and (c), (d) fuel in the average and hot channels, respectively, steady-state operation at nominal power, bottom peaked power distribution**

## COOLANT TEMPERATURE

Light water reactors such as PWR and BWR employ water as both a coolant and a moderator that slows down fast-traveling neutrons to become thermal neutrons, which are required for thermal fission reactions in the reactor core.

The coolant temperature profile, as well as the average and hot channels, are depicted in fig. 3(a). The profiles show that as the coolant enters the channels during steady-state operation, the average coolant temperature rises across the core from 300 °C to 332.1 °C, resulting in an average coolant heating rate of 32.1 °C. The average channel coolant temperature is well within thermal-hydraulic limits because it is less than the saturation temperature of the operating pressure, which is 345.32 °C. In PWR, it is necessary to prevent coolant bulk boiling.

The coolant temperature rises from 300 °C at the channel inlet to 350.1 °C at the channel outlet in the hot channel, resulting in a heating rate of 50.1 °C. The outlet temperature is higher than the saturation temperature of the operating conditions, indicating that subcooled boiling can begin somewhere in the hot channel. The difference in heating rates between the two channels is due to the hot channel having higher radial power peaking factors due to its location in the core. The fact that the result exceeds the limit in the technical data sheet for a typical reactor, tab. 1. The reason for the deviation of the obtained result from the given design limits is already mentioned in the previous case (axial power distribution-cosine peaked), as well as how to achieve a result that fits to the specified thermal limits.

## TEMPERATURES AT THE CENTERLINE, THE SURFACE OF THE FUEL, AND THE CLADDING

Figure 3(b) shows the cladding outer-surface temperature in the average and hot channels, respectively. The analysis of fig. 3(b) for the average channel shows that the cladding outer-surface temperature is equal to the coolant temperature at the inlet of the channel, then begins to increase with height and reaches its maximum value of 380.70 °C at approximately the first third of the channel then started to decrease.

The reason for the decrease in cladding temperature, as shown in fig. 3(b) has already been mentioned, where in the last part of the channel the cladding temperature arrives at the coolant temperature at the channel end.

According to the analysis of fig. 3(b), the cladding temperature profile in the hot channel has the same tendency as that in the average channel, but the maximum cladding temperature in the hot channel is recorded at the end of the first third of the channel. The maximum temperature was 414.12 °C, which is higher than the saturation temperature indicating the possibility of the subcooled boiling phenomenon. After the highest temperature point in the profile, the temperature of the cladding decreases throughout the channel, reaching to temperature degree nearly to the outlet coolant temperature at the end of the same channel.

The positions of the maximum temperatures in the channels differ, as does the time required to reach the maximum temperature. It is due to the higher radial and axial power peaking factors of the hot channel. The calculated maximum cladding temperatures in the average and hot channels differ by approximately 33.42 °C. And again, the hot channel's power generation needs to be managed in order to prevent the $q_{cr}$ and its consequences.

Figures 3(c) and 3(d) show the temperature distribution in the fuel centerline and fuel surface in the average and hot channels respectively.

In the case of the average channel, fig. 3(c) shows that the temperature profile for the centerline and fuel surface is identical to the shape of the power distribution (bottom peaked). Both profiles show that the temperature at the inlet gradually increases with height, reaching a maximum in the first third of the channel (fuel element) of 1445.39 °C and 556.09 °C, respectively. Following that, the temperature gradually began to drop to the channel outlet. Because of the power distribution, the slope of the increasing part (the part before the maximum point in the profile) is greater than that of the decreasing part (the part after the maximum point in the profile) in both profiles.

The temperature profiles in the hot channel are shaped similarly to those in the average channel, but they are higher. The maximum temperatures at the centerline and the fuel surface are 1985.17 °C and 636.85 °C, respectively. The large differences in maximum temperatures between the channels are due to the hot channel's higher radial and axial power peaking factors.

The maximum temperature recorded in the hot channel is lower than the melting temperature of the fuel (2878 20 °C) [33]. The hot channel results show that the fuel centerline, fuel surface, and cladding outer surface temperatures are all well below their limiting values for applied power distribution, indicating that the fuel and cladding temperatures are well within the thermal-hydraulic margins for power distribution. In terms of safety, changes in the composition and microstructure of the fuel caused by burnup effects should be considered when determining its melting point, as these will affect thermal conductivity in all operational states. Taking uncertainties into account, the peak fuel temperature should be lower than the fuel melting temperature by a sufficient margin to prevent the fuel from melting (see tab. 2).

## CALCULATION OF ACTUAL LOCAL $q_{act}$, CRITICAL HEAT FLUX $q_{cr}$, AND DNBR

According to the safety features of PWR, the departure from the nucleate boiling ratio is the most important parameter of the safety limits. It is the ratio of the $q_{cr}$ to the $q_{act}$ at which DNB occurs. The DNB is a complicated phenomenon influenced by a number of physical and geometrical parameters related to fuel as-

**Table 2. The effect of power distribution on thermal-hydraulic parameters**

| Parameter | Power distribution | | Reference reactor [27] | Melting temperature [°C] |
|---|---|---|---|---|
| | Cosine profile | Bottom profile | | |
| Coolant temperature [°C] (average channel) | 333 | 332.1 | 332 | – |
| Clad maximal temperature [°C] | 404.26 | 414.12 | – | 1850 °C [32] |
| Fuel centerline temperature [°C] | 1772.48 | 1985.17 | 1788 | 2878 20 °C [33] |
| MDNBR [–] | 2.1538* | 1.9872* | 1.3** | |

*Calculated under the assumption that the reference 100 % power is 112 % power
**Calculated at 112 % power (transient) [1]

sembly. In this section of the work, the DNBR values are calculated under steady-state nominal operating conditions as well as other conditions. The minimum departure from nucleate boiling ratio (MDNBR) values are determined in each case. The calculations were carried out using the physical parameters while keeping the geometrical parameters constant.

The MITH code uses a two-channel model with hot and average channels. The temperatures in the other channels, including the average channel, are lower than the temperatures in the hot channel (the hot channel has the highest temperature in the core). As a result, the hot channel parameters are thought to be reliable predictors of reactor safety. If the hot channel meets the safety limits so well, it stands to reason that the other channels will do the same. This section presents and compares the results of both channels to help the reader understand the difference between them. The DNBR and MDNBR were calculated using the hot channel results. It should be noted that the DNBR calculation was carried out under the assumption that the reference 100 % power is 112 % power (transient condition) [1].

The W-3 correlation is used in MITH code for critical heat flux $q_{cr}$ calculations. The following is the Westinghouse correlation form (W-3)

$$q_{cr} \quad q_{cr}(p,x_e,G,D_h,h_f,h_{in}) \quad K_1(p,x_e)\ K_2(x_e,G)\ K_3(x_e,D_h)\ K_4(h_f,h_{in}) \tag{1}$$

$$K_1 \quad \{(2.022 \quad 0.06238p) \quad (0.1722 \quad 0.01427p)\exp[(18.177 \quad 0.5987p)x_e]\} \tag{2}$$

$$K_2 \quad \{(0.1484 \quad 1.596x_e \quad 0.1729x_e|x_e|)2.326G \quad 3271\} \tag{3}$$

$$K_3 \quad [1.157 \quad 0.869x_e][0.2664 \quad 0.8357\exp(\quad 124.1D_h)] \tag{4}$$

$$K_4 \quad [0.8258 \quad 0.0003413(h_f \quad h_{in})] \tag{5}$$

where $q''$ [kWm$^{-2}$] is the critical heat flux $q_{cr}$, $p$ [MPa] – the pressure, $x_e$ – the local quality, $D_h$ [m] – the equivalent heated diameter, $h_f$ [kJkg$^{-1}$] – the saturated liquid enthalpy, and $h_{in}$ [kJkg$^{-1}$] – the inlet enthalpy.

For both power distributions, the code results for actual operating heat flux $q_{act}$ and $q_{cr}$ profiles are shown in figs. 4(a) and 4(b). The $q_{act}$ for the average channel is also shown to demonstrate the difference between the hot and average channels to the reader. In general, the results show that the $q_{act}$ distribution in both channels follows the distribution of applied power. The difference in heat flux between the hot and average channels is related to the hot channel's peaking factor, *i. e*. the channels are in different positions in the core, so the heat flux from the hot channel is greater than that from the average channel.

The heat fluxes $q_{act}$ and $q_{cr}$ for the symmetric power distribution are shown in fig. 4(a). Curves 1 and 2 in fig. 4(a) represent the $q_{act}$ profiles in both channels (hot and average, respectively). Curve 3 in fig. 4(a) represents the $q_{cr}$ calculated by the MITH code using the W-3 correlation equation, and line a-b in fig. 4(a) represents the position of the MDNBR value (2.1538).

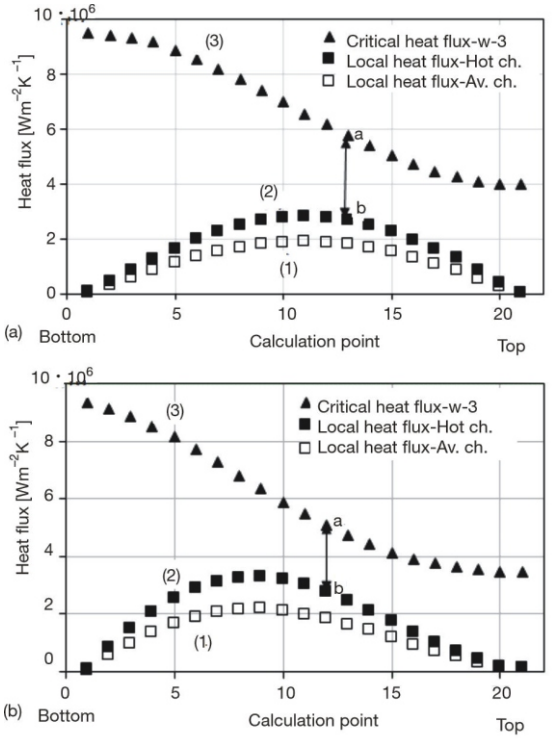


**Figure 4. The axial distribution of the critical and actual local heat flux in the hot and average channels during steady-state operation at nominal power; (a) cosine peaked power distribution and (b) bottom peaked power distribution**

The position is after the channel's midplane. Because the coolant temperature rises with height, Curve 3 decreases with distance.

In the case of a bottom peaked power distribution, heat fluxes are shown in fig. 4. (b). In fig. 4(b), Curves 1 and 2 represent the $q_{act}$ distribution in the average and hot channels, respectively. The maximum value of $q_{act}$ is located in the same location in both channels, in the lower part of each channel.

The heat fluxes ($q_{act}$ and $q_{cr}$) for the bottom peaked power distribution are shown in fig. 4(b). Curves 1 and 2 in fig. 4(a) represent the $q_{act}$ profiles in both channels (hot and average, respectively).

Curve 3 in fig. 4(b) depicts the $q_{cr}$ calculated by MITH code using the W-3 correlation. The position of the MDNBR value (1.987) along the channel is represented by lines a-b. MDNBR is measured in the lower half of the channel height. Curve 3 continues to decrease with height as the coolant temperature rises from point to point along the channel.

The MDNBR values obtained in both cases of power distribution are well within the thermal-hydraulic limits given in the datasheet of the tested reactor [27]. The standard material temperature limits are taken into account, $T_{clad}$ 800 °C for Zircaloy-4 cladding, and the fuel is not allowed to reach its melting point of 2878 20 °C (tabs. 1 and 2). Although zirconium has a melting point of 1850 °C, zirconium alloys are not suitable for use at extremely high temperatures. At 810 °C, zirconium starts to undergo a phase change from a close-packed hexagonal structure to a body-centered cubic structure, and it is critical to maintaining below this temperature. At these temperatures, a reaction with $UO_2$ can occur at the zirconium cladding inner interface. At the temperatures and stresses typical of PWR reactor design, zirconium alloys exhibit significant creep. Creep rates increase significantly with increasing temperature and are accelerated by reactor irradiation. Zirconium chemically reacts with steam at high temperatures (above 800 °C) to produce hydrogen in an exothermic reaction. This reaction must be taken into account when evaluating any LOCA event that may expose the fuel elements to steam. For the reasons stated, the cladding temperature should not exceed 800 °C to maintain nuclear power plant safety limits [32-35].

The hot channel code analysis in this work demonstrates that the maximum cladding temperature and maximum fuel centerline temperature are both below the limits. The core exit temperature $T_{out}$ is significantly lower than the coolant limit (saturation temperature of operating pressure). In PWR, the coolant's thermal limit is the operating pressure's saturation temperature. Based on the results and discussions, we can conclude that the tested reactor meets the steady-state thermal-hydraulic constraints.

Figures 5(a) and 5(b) show the variation of DNBR with channel height (b). The power distribution affects the DNBR distribution along the channel. Regardless of the power distributions used, the maximum values of DNBR are recorded at the channel's inlet and outlet, while the lower values, including MDNBR, are recorded in the distance between the inlet and outlet of the channel. Figure 5(b) shows the MDNBR position by enlarging the bottom parts of the curves in fig. 5(a). The MDNBR position is logically dependent on the power distribution. Because of the effect of increasing fluid enthalpy on decreasing CHF, the MDNBR occurs downstream from the maximum heat flux position fig. 4(a,b) and fig. 5(b).

## OPERATING CONDITIONS AND THERMAL-HYDRAULIC PERFORMANCE

To evaluate the thermal-hydraulic performance of the PWR, a steady-state hot channel analysis (HCA) for a variety of operating conditions was performed by investigating the thermal-hydraulic parameters under different operating conditions. The MDNBR, maximum fuel and cladding temperatures, core exit temperature, and pressure drop at various power distributions, power levels, and mass-flow rates (in $kgs^{-1}$) were investigated. For the hot channel analysis, the thermal-hydraulic constraints shown in tabs. 1 and 2 are used for comparison. Tables 3 and 4 show the re-

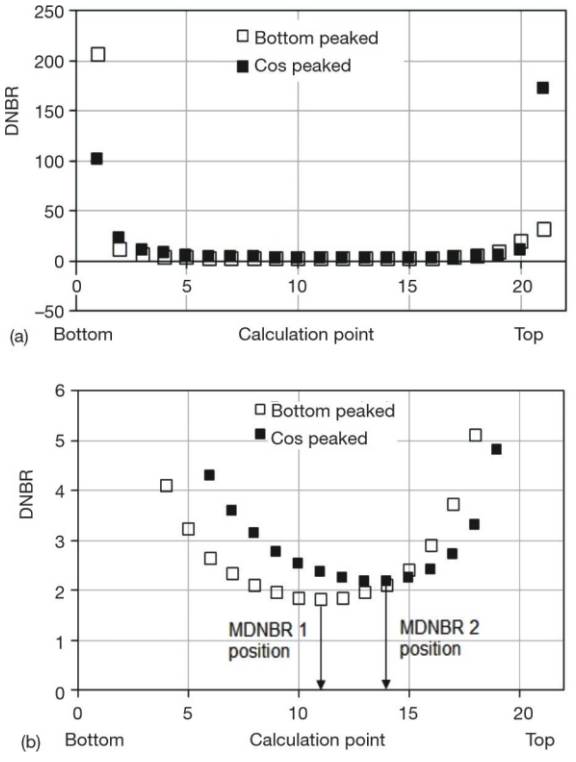


**Figure 5. Influence of power shape on DNBR distribution in the hot channel; (a) DNBR is calculated using W-3 correlation for cosine and bottom peaked power distribution and (b) enlarging the bottom parts of the DNBR's curves in (a)**

**Table 3. The effect of operating power level and mass-flow rate on thermal-hydraulic parameters (bottom peaked power distribution)**

| Power [%] | Flow rate [%] | Hot channel temperature [°C] | | | MDNBR | $p$ [Psi] | $q_{cr}$ $10^6$ [$Wm^{-2}K^{-1}$] | $q_{act}$ $10^6$ [$Wm^{-2}K^{-1}$] |
|---|---|---|---|---|---|---|---|---|
| | | Cladding | Fuel | | | | | |
| | | | Surface | Centerline | | | | |
| 100 | 100 | 414.12 | 636.86 | 1985.17 | 1.9872 | 10.99 | 5.6783 | 2.6347 |
| 100 | 90 | 415.05 | 636.86 | 1985.17 | 1.7988 | 9.92 | 4.7357 | 2.6347 |
| 110 | 100 | 420.02 | 709.92 | 2158.87 | 1.7095 | 10.02 | 4.9628 | 2.8959 |
| 110 | 90 | 420.90 | 711.27 | 2158.89 | 1.5233 | 10.23 | 4.412 | 2.8959 |

**Table 4. The effect of operating power level and mass-flow rate on thermal-hydraulic parameters (cosine peaked power distribution)**

| Power [%] | Flow rate [%] | Hot channel temperature [°C] | | | MDNBR | $p$ [Psi] | $q_{cr}$ $10^6$ [$Wm^{-2}K^{-1}$] | $q_{act}$ $10^6$ [$Wm^{-2}K^{-1}$] |
|---|---|---|---|---|---|---|---|---|
| | | Cladding | Fuel | | | | | |
| | | | Surface | Centerline | | | | |
| 100 | 100 | 404.26 | 605.11 | 1772.48 | 2.1538 | 10.84 | 5.048 | 2.3451 |
| 100 | 90 | 404.86 | 605.09 | 1772.48 | 1.9205 | 9.73 | 4.5085 | 2.3451 |
| 110 | 100 | 410.64 | 652.27 | 1911.12 | 1.8216 | 10.85 | 4.7016 | 2.5779 |
| 110 | 90 | 411.74 | 625.54 | 1911.22 | 1.6106 | 9.93 | 4.1565 | 2.5779 |

sulting MDNBR values for various operating conditions.

It is essential to consider different operating conditions and $q_{cr}$ correlations when calculating core parameters for an accurate set of properties [36]. However, only the W-3 correlation was used in this study. Tables 3 and 4 show that even in the worst case of operation, 110 % overpower and 90 % mass-flow rate, the obtained MDNBR value is well within the US Nuclear Regulatory Commission (NRC) limits (MDNBR 1.3 at 112 % power-transient condition) [1, 36].

Regardless of power distribution configuration (cosine or bottom peaked), higher core power and lower flow rate levels promote higher surface heat flux in the core, lowering MDNBR in the hot channel. Tables 3 and 4 show that the temperatures of the fuel centerline, fuel surface, and cladding outer surface are increased but remain below the temperature limits. The pressure drop was not too erratic. The obtained result is in good agreement with the reference data under these operating conditions, tab. 1. The temperatures of the fuel (centerline and surface) and the cladding are more sensitive to the power level than to the mass flow rate in both cases of power distribution.

In terms of heat flux, the $q_{act}$ behaves similarly to the temperature of the fuel and cladding. It makes sense because the $q_{act}$ is directly proportional to the temperatures of the fuel and cladding. The $q_{cr}$, on the other hand, is a function of many parameters, including exit quality, inlet enthalpy, saturation enthalpy, and mass flux. All of these factors are affected by the power level, power distribution, and mass-flow rate. As a result, the $q_{cr}$ is highly sensitive to changes in power level and mass-flow rate.

Because pressure is an important parameter for PWR thermal-hydraulic performance, the code calculates pressure drop as one of the thermal-hydraulic parameters. In a hot and average channel, the total pressure drop is the sum of the pressure drops caused by spacers and friction.

Equation (6) is used to calculate the resistance of spacers

$$P_{\text{spacer}} \quad P_{\text{total with spacer}} \quad P_{\text{total with spacer}} \tag{6}$$

The pressure drop at the spacer grid is related to the fluid velocity $V_b$ in the rod bundle (the subscript $b$ indicates the bundle)

$$P_s \quad C_D \frac{\rho}{2} V_b^2 \tag{7}$$

where $C_D$ is the drag coefficient of the spacer grid and $\rho$ is the fluid density.

The Reynolds number $Re_b$ of the flow in the rod bundle is expressed as

$$Re_b \quad \frac{V_b D_h}{v} \tag{8}$$

with $D_h$ the hydraulic diameter ($D_h = 4A/S$), where $A$ is the flow cross-section, $S$ – the wetted perimeter, and $v$ – the kinematic viscosity.

The frictional pressure drop can be calculated using

$$P_f \quad f \frac{\rho}{2} V_b^2 \frac{L}{D_h} \tag{9}$$

where $f$ is the friction factor, $\rho$ [$kgm^{-3}$] – the fluid density, $V_b^2$ [$ms^{-1}$] – the velocity, $L$ [m] – the channel length, and $D_h$ [m] – the hydraulic diameter.

For smooth pipes, Blasius (1913) has shown that the friction factor (in a range of $3.000 < Re < 100.000$) could be computed by

$$f \quad \frac{0.079}{Re^{0.25}} \quad 3000 \quad Re \quad 100000 \tag{10}$$

However, in the case of $Re > 10^5$, the following equation is found to be more accurate

$$f \quad \frac{0.046}{\mathrm{Re}^{0.20}} \tag{11}$$

In the code, the previous formulas were used to show the relationship between pressure drops, mass-flow rate, power distribution, and operating power level. The effect of these parameters on total pressure drops was investigated by calculating total pressure drops with various values of each parameter while holding the other geometrical and hydrodynamic parameters constant. Tables 3 and 4 show the outcomes. The results show a strong relationship between the tested parameters and total pressure drop.

There must be no melting of the fuel or cladding and a low-fission gas release for safe operating conditions. According to the literature, the fission gas can be kept lower during steady-state operation by limiting the average fuel temperature to 1673 K and the cladding outer surface temperature to 1000 K (for zircaloy -4). It is thought that imposing a 3123 K peak fuel centerline temperature is more limiting than imposing an average fuel temperature constraint [ 27, 36]. Tables 3 and 4 show that the surface fuel, fuel centerline, and cladding outer surface temperatures in the hot channel are below their limiting values for all test operating power and flow rate cases [1, 25, 36].

## CONCLUSIONS

A steady-state thermal-hydraulic study was conducted using 1-D computer code to investigate the high power density pressurized water reactor PWR and identify the main thermal-hydraulic challenges that characterize this reactor. Maximum fuel and cladding surface temperatures, maximum surface heat flux, MDNBR, and maximum core exit temperature have all been determined to be within safe limits. Even when the power is increased by 10 % of the nominal operating power and the mass flux is reduced by 10 % of the total mass flux, the thermal-hydraulic parameters satisfy the thermal-hydraulic constraints. In general, the calculation shows that control over power generation in the hot channel is required in our tested reactor to guarantee reactor safety. Furthermore, the total pressure drop in the core is less than the safe limit.

The high level of agreement between the obtained results and the data from the referenced reactor demonstrates the code's validity and efficiency (PWR-W). The minor discrepancies could be explained by differences in the relevant physical parameters used in each method of calculation. Furthermore, we can ensure that all thermal-hydraulic safety parameters are within the thermal design limits for steady-state operating conditions. As a result, it is concluded that the referenced reactor (PWR-W) is safe to operate under the aforementioned tested operating conditions and remains within the thermal design limits.

## ACKNOWLEDGMENT

The first author would like to express his heartfelt appreciation and gratitude to Eng. Mohamed Banour (M.Sc.) and Eng. Khamis Al-Thuibi (M.Sc.) at Tajoura Center for Nuclear Research – Tripoli, Libya, for their invaluable assistance. His appreciation also goes to Dr. Zoltan Hozer, head of the nuclear fuel department at Hungary's Center for Energy Research (CER) Budapest, for his insightful comments. TonyTakács' English improvements are gratefully acknowledged by the first author. The first author would also like to thank Tajoura Nuclear Research Centre (Tripoli, Libya) for providing the code and allowing him to use their computer system network.

## AUTHORS' CONTRIBUTIONS

The first author performed and wrote all calculations and analyses, while the second author provided the idea, supervised, and controlled the project work content. The first author wrote, reviewed, and supervised the manuscript. The first author is responsible of the manuscript's content.

## REFERENCES

[1] Todreas N. E., Kazimi, M. S., Nuclear Systems I – Thermal Hydraulics Fundaments, Taylor&Francis, USA, 1993, pp. 19-71, http://www.gammaexplorer.com/wp-content/uploads/2014/03/Nuclear-Systems-I-Thermal-Hydraulic-Fundamentals-Todreas-1.pdf.

[2] Tong, L. S., Weisman, J., Thermal Analysis of Pressurized Water Reactor, La Grange Park, Illions, American Nuclear Society, USA, 3rd edition, 1996, pp. 30-614, ID: 300028|ISBN: 978-0-89448-038-6

[3] Hutli, E., Kridan, R., Thermal-Hydraulic Analysis of Light Water Reactors Under Different Steady-State Operating Conditions, Part 1-Boiling Water Reactor, *Nucl Technol Radiat, 37* (2022), 4, pp. 259-275

[4] Akbari, R., *et al*., Thermal-Hydraulics Analysis of Pressurized Water Reactor Core by Using Single Heated Channel Model, *Journal of Applied and Computational Mechanics, 3* (2017), 3, pp. 192-198

[5] Mesquita, A. Z., Experimental Heat Transfer Analysis of the IPR-R1 TRIGA Reactor, International Conference on Research Reactors, Safe Management, and Effective Utilization, IAEA-CN-156/S-26, Sydney Australia 2007, https://inis.iaea.org/collection/NCLCollectionStore/_Public/39/043/39043136.pdf?r=1

[6] Helmy, S., *et al.*, Analysis of Thermal Hydraulic Behavior of KONVOI PWR During a Design Extension Condition, *Nucl Technol Radiat, 36* (2021), 1, pp. 1-11

[7] Mukin, R., *et al.*, Subchannel Modeling of Single Rod Bowing in a Bundle Geometry, *Nuclear Engineering and Design, 340* (2018), pp. 347-369

[8] Khedr, A., Thermal-Hydraulic Fortran Program for Steady-State Calculations of Plate-Type Fuel Research Reactors, *Nucl Technol Radiat, 23* (2008), 1, pp. 19-30

[9] Mylonakis, A. G., *et al.*, Multi-Physics and Multi-Scale Methods Used in Nuclear Reactor Analysis, *Annals of Nuclear Energy, 72* (2014), Oct., pp. 104-119

[10] Sharma, D., Pandey, K. M., Different Codes used for Reducing Thermal Hydraulics Problems in Nuclear

Reactors: a Review, *International Journal of Advance Research in Science and Engineering, 4* (2015), pp. 89-101
[11] Hutli, E., *et al.*, Experimental Approach to Investigate the Dynamics of Mixing Coolant Flow in Complex Geometry Using PIV and PLIF Techniques, *Thermal Science Scientific Journal, 19* (2015), 3, pp. 989-1004
[12] Hutli, E., *et al.*, Experimental and Numerical Investigation of Coolant Mixing in a Model of Reactor Pressure Vessel Down-Comer and in Cold Leg Inlets, *Thermal Science Scientific Journal, 21* (2017), 3, pp. 1491-1502
[13] Farkas, I., *et al.*, The Applicability of CFD to Simulate and Study the Mixing Process and the Thermo-Hydraulic Consequences of a Main Steam Line Break in PWR Model, *Thermal Science International Scientific Journal, 21* (2017), 6B, pp. 3025-3036
[14] Hiroyuki, Y., *et al.*, Numerical Evaluation of Fluid Mixing Phenomena in Boiling Water Reactor Using Advanced Interface Tracking Method, *Journal of Fluid Science and Technology, 3* (2008), 2, pp. 311-322
[15] Ezsol, G., *et al.*, Measurements for Verification and Validation of Thermal-Hydraulic Computer Code Used for Thermal-Hydraulic Analysis of VVER440 Typical Fuel Assembly, *Measurement, 171* (2021), 108787, https://doi.org/10.1016/j.measurement.2020.108787
[16] Farkas, I., *et al.*, Validation of Computational Fluid Dynamics Calculation Using Rossendorf Coolant Mixing Model Flow Measurements in Primary Loop of Coolant in a Pressurized Water Reactor Model, *Nuclear Engineering and Technology, 4* (2016), 4, pp. 941-951
[17] Imke, U., Sanchez, V., Validation of the Subchannel Code SUBCHANFLOW Using the NUPEC PWR Tests (PSBT), Hindawi Publishing Corporation, *Science and Technology of Nuclear Installations*, (2012), pp. 1-12, doi:10.1155/2012/465059, https://downloads.hindawi.com/journals/stni/2012/465059.pdf
[18] ***, Progress of the DUPIC Fuel Compatibility Analysis (II)-Thermal-Hydraulics Korea Atomic Energy Research Institute (KAERI/TR-2965/2005), 2005, https://www.osti.gov/etdeweb/servlets/purl/20710103
[19] ***, SCIENTECH Inc., RELAP5/Mod3 Code Manual, Vol. (IV): Models and Correlations, Idaho, March, NUREG/CR-5535, (1998), https://www.nrc.gov/docs/ML1103/ML110330271.pdf
[20] Basile, D., *et al.*, COBRA-EN: An Upgraded Version of the COBRA-3C/MIT Code for Thermal-Hydraulic Transient Analysis of Light Water Reactor Fuel Assemblies and Cores. Report 1010/1, ENELCRTN, Milano, 1999, https://inis.iaea.org/search/search.aspx?orig_q=RN:41021764
[21] ***, CASL, COBRA-TF Subchannel Thermal-Hydraulics Code (CTF) Theory Manual [R], USA: Pennsylvania State University, 2015, http://www.casl.gov/
[22] Kaminaga, M., COOLOD-N A Computer code, for the Analyses of Steady-state Thermal-hydraulic in Plate-Type Research Reactors, Japan Atomic Energy Research Institute, Ibaraki-ken & Japão, 1990, https://inis.iaea.org/collection/NCLCollectionStore/_Public/21/072/21072811.pdf?r=1
[23] Hainoun A., Ghazi N., Abdul-Moaiz B.M., Safety Analysis of the IAEA Reference Research Reactor During Loss of Flow Accident Using the Code MERSAT, *Journal of Nuclear Engineering and Design, 240* (2010), 5, pp. 1132-1138
[24] Carajilescov, P., Bastos, Experimental Analysis of Pressure Droop and Flow Redistribution in Axial Flows in Rod Bundles, *Journal of Brazilian Society of Mechanical Sciences, 22* (2000), pp. 599-612 https://www.scielo.br/scielo.php?pid=S0100-73862000000400009&script=sci_abstract
[25] Castellanos, D. A., *et al.*, Thermal-Hydraulic Code for Estimating Safety Limits of Nuclear Reactors with Plate Type Fuels, International Nuclear Atlantic Conference – INAC, Belo Horizonte, MG, Brazil, Associacao Brasileira De Energia Nuclear – Aben, 2017
[26] Guo, J., *et al.*, Coupled Neutronics/Thermal-Hydraulics Analysis of a Full PWR Core Using RMC and CTF, *Annals of Nuclear Energy, 109* (2017), Nov., pp. 327-336
[27] Duderstadt, J. J., Hamiltom, L. J., Nuclear Reactor Analysis, John Wiley & Sons, Inc, USA, 1976, Appendix H, pp. 634-635
[28] Pinem, S., *et al.*, Reactivity Coefficient Calculation for AP1000 Reactor Using the NODAL3 Code, Journal of Physics: Conference Series, 962, International Conference on Nuclear Technologies and Sciences (ICoNETS 2017) Makassar, Indonesia, 2017, pdf (iop.org)
[29] Basma Foad, B., Abdel-Latif, S. H., Takeda, T., Reactivity Feedback Effect on Loss of Flow Accident in PWR, *Nuclear Engineering and Technology, 50* (2018), pp. 1277-1288, https://doi.org/10.1016/j.net.2018.07.012
[30] Cheng, L.Y., Cuadra, A., Brown, N., PWR Plant Model to Assess Performance of Accident Tolerant Fuel in Anticipated Transients and Accidents, *Nuclear Science & Technology Department Brookhaven National Laboratory U.S. Department of Energy Office of Fuel Cycle Technologies, USA* (2014), pp. 1-19, 87933.pdf (bnl.gov)
[31] ***, IAEA, Computational Analysis of the Behavior of Nuclear Fuel under Steady State, Transient and Accident Conditions, IAEA-TECDOC-1578, 2007, https://www-pub.iaea.org/MTCD/Publications/PDF/TE_1578_web.pdf
[32] ***, ATI Inc. (Allegheny Technologies Incorporated), Zirconium Alloys, Reactor Grade Zirconium, *Technical Data Sheet, Version, 1* (2015), pp. 1-3, https://www.atimaterials.com/Products/Documents/datasheets/zirconium/alloy/Zr_nuke_waste_disposal_v2.pdf
[33] ***, U. S. Department of Energy Office of Environmental Management, Depleted Uranium Hexafluoride Management Program, Characteristics of Uranium and Its Compounds, *Depleted Uranium Hexafluoride Fact Sheet,* (2001), pp. 1-4, https://web.evs.anl.gov/uranium/pdf/UraniumCharacteristicsFS.PDF
[34] Popov, N. K., Thermal-Hydraulic Design Fundamentals, *The Essential CANDU- a Textbook on the CANDU Nuclear Power Plant Technology, Chapter 6* (2017), pp. 59-106
[35] Todreas, N. E., Kazimi, M. S., Nuclear Systems Volume 1: Thermal Hydraulic Fundamentals, CRC Press, Boca Raton, FL, USA, 2012
[36] Alam, S. B., Lindley, B. A., Parks, T. G., Hot Channel Analysis of a 333 $MW^{th}$ Civil Nuclear Marine Core using the Cobra-En Code, $16^{th}$ International Topical Meeting on Nuclear Reactor Thermal Hydraulics (NURETH-16), USA, Chicago, IL, 2015, pp. 5900-5913 http://glc.ans.org/nureth-16/data/papers/12972.pdf

Received on June 17, 2022
Accepted on November 28, 2022

**Ездин ХУТЛИ, Рамадан КРИДАН**

## ТЕРМОХИДРАУЛИЧНА АНАЛИЗА ЛАКОВОДНОГ РЕАКТОРА У СТАБИЛНИМ РАДНИМ УСЛОВИМА
### Други део – реактор са водом под притиском

Једнодимензионални рачунарски MITH програм коришћен је у овом раду за извођење потканалних термохидрауличних анализа типичног Вестингхаусовог модела реактора са водом под притиском. Два карактеристична канала, врући и просечни, са истим протоком и падом притиска, тестирана су у стационарним радним условима. У овој анализи, канал са највишом температуром је означен као врући канал. За прорачуне модел канала је подељен на 20 делова. На термохидрауличне перформансе тестираног реактора утицали су расподела снаге, ниво снаге и проток масе расхладне течности. Добијени су профили расподеле температуре горивног елемента и хладиоца за просечни и врући канал. Такође је извршена анализа критичног топлотног флукса и израчунати су топлотни флуксеви у оба канала. Корелација W-3 коришћена је за испитивање критичног топлотног флукса у најтоплијем каналу. Неки подаци из листе за типични реактор са водом под притиском коришћени су као улазни подаци, док су други коришћени за валидацију кода. Програм је верно репродуковао резултате Вестингхаусовог модела реактора, укључујући температуре хладиоца, кошуљице, средишње линије и површине горива, квалитет и локални топлотни флукс и коефицијент минималног одступања од кључања.

*Кључне речи: гориво, кошуљица, хладилац, температура, притисак, топлотни флукс, одступање од кључања језгра*